MATERIALS SCIENCE

Living microecological hydrogels for wound healing

Guopu Chen[1], Fengyuan Wang[2], Xiaoxuan Zhang[2], Yixuan Shang[1], Yuanjin Zhao[1,2,3]*

Chronic hard-to-heal wounds draw great attention worldwide, as their treatments are limited by infections and hypoxia. Inspired by the natural oxygen production capacity of algae and the competitive advantage of beneficial bacteria over other microbes, we presented a living microecological hydrogel (LMH) with functionalized *Chlorella* and *Bacillus subtilis* encapsulation to realize continuous oxygen delivery and anti-infections for promoting chronic wound healing. As the hydrogel consisted of thermosensitive Pluronic F-127 and wet-adhesive polydopamine, the LMH could keep liquid at a low temperature while quickly solidifying and tightly adhering to the wound bed. It was demonstrated that by optimizing the proportion of the encapsulated microorganism, the *Chlorella* could continuously produce oxygen to relieve hypoxia and support the proliferation of *B. subtilis*, while *B. subtilis* could eliminate the colonized pathogenic bacteria. Thus, the LMH substantially promoted the healing of infected diabetic wounds. These features make the LMH valuable for practical clinical applications.

INTRODUCTION

Chronic hard-to-heal wounds are considered as those that fail to heal by 40 to 50% after over 4 weeks of standard management, including diabetic ulcers, pressure sores, etc. Treatment of a chronic hard-to-heal wound and its therapeutic impediments have always attracted great concern in health care and medical fields, bringing about substantial economically challenging burdens worldwide (*1*–*5*). Hypoxia and infection are two non-negligible issues during the occurrence, development, and prognosis of chronic wound healing (*6*–*10*). Hypoxia, caused by ischemia, can lead to insufficient oxidative energy supply, low metabolism, and dysfunction of inflammatory cells and repair cells. Besides, as a subsequent symptom of hypoxia, multiple pathogen infections may occur because of nerve malnutrition and decreased body resistance, which could result in tissue apoptosis and persistent inflammation (*11*–*13*). Generally, the degree of hypoxia and infection would be further aggravated owing to the inappropriate coverage of commonly used wound dressings in clinical wound management. To address these, strategies integrated with oxygen supply or antibiosis have been developed, including wound irrigation, antibacterial agents, hyperbaric oxygen chamber, etc. (*14*–*16*). Although with many successes, the oxygen supply of existing devices can only last for a short time, restricting their practical performance. In addition, because of the highly plastic genome and rapid reproduction abilities of the bacteria, they can rapidly mutate and develop resistance to chemicals, resulting in limited control effect of antibacterial drugs on bacterial pathogens (*17*, *18*). Moreover, most of the present clinical therapies are limited by frequent administration and high costs. Therefore, a simple and effective wound therapy that can continuously deliver oxygen and hinder the emergence of drug resistance is still demanded.

Here, inspired by the natural oxygen production capacity of algae and the competitive advantage of beneficial bacteria over other microbes, we exhibited a living microecological hydrogel (LMH) encapsulated with both functionalized algae and bacteria for promoting wound healing (Fig. 1). In nature, algae can constantly produce abundant oxygen through photosynthesis with the existence of sunshine, providing dissolved oxygen for the survival of other underwater organisms and contributing to most of the oxygen on earth (*19*, *20*). However, these algae are usually difficult to be directly used as oxygen suppliers for wounds because their proliferation would be inhibited by pathogenic bacteria contamination in the wound bed. In contrast, the naturally predominant bacteria can effectively eradicate colonization of pathogenic bacteria through rapid mass reproduction to occupy the living space, as well as secreting abundant antimicrobial agents to enhance racial competitiveness (*21*–*24*). Nonetheless, their bacteriostatic effect is limited by insufficient oxygen supply when proliferating to a certain degree in the wound bed. Thus, it is conceived that by simultaneously using oxygen-produced algae and antimicrobial beneficial bacteria in a hydrogel with a certain balance, a common natural LMH system would be developed for effective wound treatment.

In this research, we encapsulated living algae and probiotic bacteria into the thermoplastic hydrogel to realize continuous oxygen delivery and anti-infection for rapid healing of infected diabetic wounds. The algae in the system is *Chlorella pyrenoidosa*, as it has been widely used in the food industry, skincare, and biomedicines (*25*, *26*), while the beneficial bacterial component was *Bacillus subtilis*, which is routinely colonized on the body surface and used in clinical oral capsules (*27*–*30*). The hydrogel consisted of thermosensitive Pluronic F-127 and wet-adhesive polydopamine (PDA) (*31*–*34*). Benefitting from the near–to–body temperature lower critical solution temperature of Pluronic F-127 (*35*–*38*), the mixed hydrogel could keep liquid form at low temperature while quickly solidifying on the body wound bed. In addition, because of the flexibility and adhesion ability of the additive PDA (*39*–*43*), the hydrogel could well suit the skin and tightly adhere to the skin wound. It was demonstrated that by optimizing the proportion of living algae and probiotic bacteria, they both could well survive and display functions. Thus, the LMH showed desirable promoting wound repair

[1]Department of Burns and Plastic Surgery, Institute of Translational Medicine, The Affiliated Drum Tower Hospital of Nanjing University Medical School, Nanjing 210002, China. [2]Department of Dermatology, Zhongda Hospital, School of Biological Science and Medical Engineering, Southeast University, Nanjing 210096, China. [3]Oujiang Laboratory (Zhejiang Lab for Regenerative Medicine, Vision and Brain Health), Wenzhou Institute, University of Chinese Academy of Sciences, Wenzhou, Zhejiang 325000, China.
*Corresponding author. Email: yjzhao@seu.edu.cn

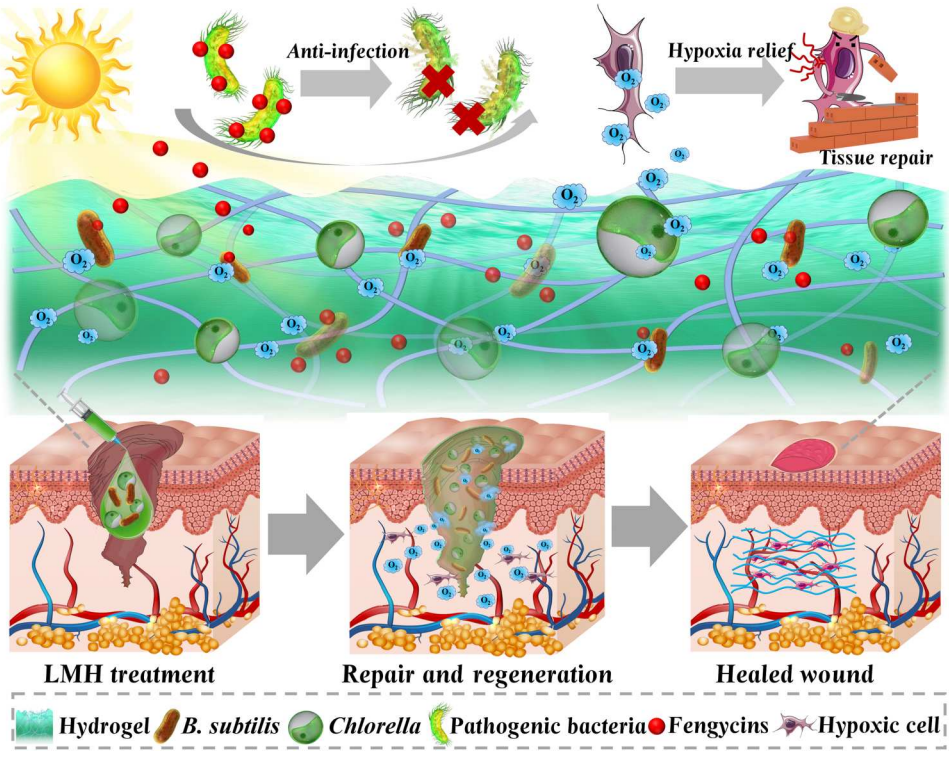

Fig. 1. Schematic illustrations of application of the LMH for hard-to-heal wounds. LMH was constructed by simultaneously using oxygen-produced *Chlorella* and antimicrobial beneficial *B. subtilis* into a hydrogel. The microecological hydrogel could fill the wound bed. The *Chlorella* in the microecological hydrogel could produce oxygen to enhance survival of the *B. subtilis* and relieve hypoxia, while the *B. subtilis* could control infections through releasing antimicrobial agents. The LMH could heal the infected diabetic wound using an antibacterial and by relieving hypoxia.

capability in treating the infected diabetic wounds. These results indicated that the LMH is valuable in treating practical chronic wounds and promising for other disease treatments.

RESULTS

In a typical experiment, an LMH with functionalized algae and bacteria encapsulation was designed, which could continuously deliver oxygen and antibacterial substances into chronic hard-to-heal wound beds (Fig. 2A). The biomaterial covering on the wound bed should have low viscosity at room temperature while rapidly gelatinizing upon administration. Therefore, thermosensitive Pluronic F-127 triblock copolymers and PDA were used to encapsulate *Chlorella* and *B. subtilis*, which could be gelled at body temperature (Fig. 2, B and C). The gelation time of different concentrations of simple Pluronic F-127 was evaluated after heating from room temperature to 37°C (Fig. 2D and fig. S1). It was found that the gelation time decreased with the increasing Pluronic F-127 concentration. The low concentration of 15% spent over 15 min to gel, while the high concentration of 20% gelled within a few seconds. A moderate gelation time of about 1 min was chosen with a concentration of 18%.

To enhance anchoring strength between hydrogel and wound bed, the mussel-bioinspired PDA was introduced into the Pluronic F-127 hydrogel. The addition of PDA could shorten the gelling time of Pluronic F-127, while *Chlorella* and *B. subtilis* slightly prolonged the gelling time (Fig. 2E and fig. S2). This phenomenon may be ascribed to the hydrogen bond formed between the hydroxide radical in both Pluronic F-127 and PDA and the introduction of the PDA network. The storage modulus changes of simple Pluronic F-127, Pluronic F-127 with PDA, *Chlorella*, or *B. subtilis* addition were further tested by rheology, and obvious sol-to-gel transition could be observed at phase transition temperature (fig. S3). With the thermosensitive gelation ability of Pluronic F-127 and the wet-adhesive ability of PDA, the hybrid hydrogel could be written directly in warm water (fig. S4). Furthermore, intergrowth of the *Chlorella* and *B. subtilis* could be observed within the three-dimensional (3D) network structure of the hybrid hydrogel (figs. S5 and S6). Upon injecting the pre-gel solution into the wound bed, the abundant catechol group in the hydrogel network showed enhanced adhesive affinity to nucleophiles on the wound surface, and the adhesive force increased with the increasing concentration of PDA (fig. S7).

To realize the ecological equilibrium of the LMH, the proliferation rate of *Chlorella* and *B. subtilis* in the hydrogel with different concentrations of PDA was evaluated. A faster rate of proliferation was observed in both *Chlorella* and *B. subtilis* when the concentration of the PDA increased, as the PDA could provide a matrix for cellular attachment and enhance the adhesion between the microorganism and the hydrogel (Fig. 3, A to C). Considering the results of gelation time, adhesion force, and proliferation rate, the concentration of PDA was set as 1%. The resultant LMH could adhere tightly to the surface of human skin (fig. S8). The proliferation of *Chlorella* under different light and with or without hydrogel

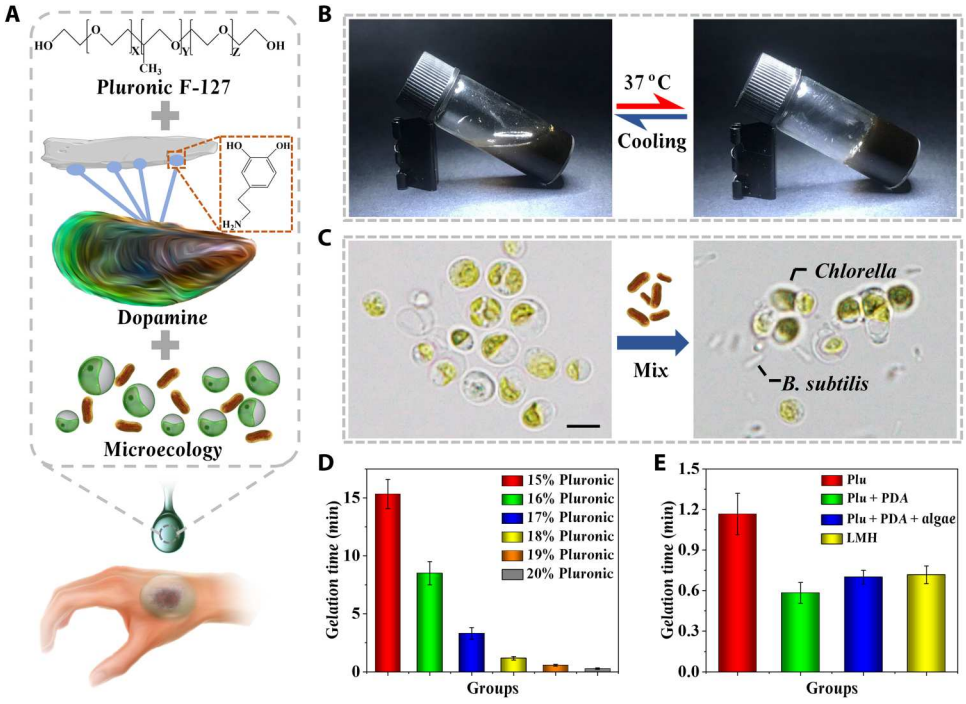

Fig. 2. Preparation and characterization of the LMH. (**A**) Schematic illustrations of the composition of the LMH. (**B**) LMH maintained liquid at room temperature of 25°C and gelled at body temperature of 37°C. (**C**) Hydrogel loaded with simple *Chlorella* or both *Chlorella* and *B. subtilis*. (**D**) Gelation time of different concentrations of simple Pluronic hydrogel at 37°C. (**E**) Gelation time of simple 18% Pluronic hydrogel, 18% Pluronic hydrogel mixed with PDA, 18% Pluronic hydrogel mixed with PDA and algae, and LMH. Scale bar, 5 μm (C). $n = 3$ per group (D and E).

encapsulation was also tested (Fig. 3D). It could be observed that the algae proliferated better under white light, and the hydrogel encapsulation might limit the proliferation rate. The oxygen could be produced by *Chlorella* through light reactions (fig. S9). Dissolved oxygen produced by algae loaded in the hydrogel showed almost no difference from that of the simple algae (Fig. 3E), and almost no difference in oxygen production was observed between *Chlorella* encapsulated in Pluronic F-127 with or without the addition of PDA under the used illumination intensity and thickness of the hydrogel (fig. S10). This phenomenon may be ascribed to the enhanced oxygen production capacity after encapsulation and the more convenient release from the 3D structure of the hydrogel.

In addition, the ratio between *Chlorella* and *B. subtilis* was evaluated. The algae (10^7 cells/ml) were cocultured with different concentrations of *B. subtilis*, and no influence could be observed when the concentration of *B. subtilis* was limited to 10^7 cells/ml (Fig. 3, F and G). However, obvious death of *Chlorella* appeared when the concentration of *B. subtilis* reached 10^8 cells/ml. The superfluous *B. subtilis* may accelerate the consumption of dissolved oxygen, and the residual oxygen could not support the aerobic respiration of *B. subtilis* and *Chlorella*. Furthermore, *B. subtilis* (10^7 cells/ml) were cocultured with different concentrations of algae. The proliferation rate of *B. subtilis* increased with the increased concentration of *Chlorella* because the algae can produce nutrients and oxygen through light reactions, which is beneficial for the proliferation of bacteria (Fig. 3, H and I). Therefore, considering the results of coculture, *B. subtilis* (10^7 cells/ml) and *Chlorella* (10^7 cells/ml) were loaded into the LMH for the following experiments.

To prove the application value of the LMH in the treatment of hard-to-heal wounds, the in vitro antibacterial ability of the LMH was tested by disc diffusion method. *Staphylococcus aureus* is the most important factor in wound infections. Therefore, the representative Gram-positive *S. aureus* was spread on the nutrient agar plate. Afterward, the *B. subtilis* solutions were dropped onto the paper filter discs with a diameter of 6 mm. The simple hydrogel without *B. subtilis* and *Chlorella* encapsulation, living bacterial hydrogel (LBH) with only *B. subtilis* encapsulation, and LMH were molded into the same size. They were placed onto the center of a plate and incubated at 37°C for 24 hours. A distinct inhibition zone could be formed between the *B. subtilis* and *S. aureus* (Fig. 4A). No inhibition zone was observed in the hydrogel alone, while the LBH exhibited obvious antibacterial activity, which could be enhanced with the addition of *Chlorella* (Fig. 4B and fig. S11). The antibacterial efficiency of LMH against *S. aureus* was further identified by colony counting method. During coculture of 3 days with LMH, the viability of *S. aureus* observed greatly reduced (figs. S12 and S13). The phenomenon may be ascribed to the fact that the fengycins secreted by *B. subtilis* can eliminate *S. aureus* by inhibiting *S. aureus* quorum sensing (*44*). Furthermore, a large number of *B. subtilis* were observed crawling out from the paper filter disc, while virtually no bacteria escaped from the hydrogel. These results indicated that the LMH could serve as an antibacterial and minimize the potential risk of secondary bacterial infections.

Wound healing is a process involving multiple cells at the same time, including fibroblast proliferation and vascular endothelial cell migration and differentiation, which may be seriously affected by tissue hypoxia. Therefore, human umbilical vein endothelial cells

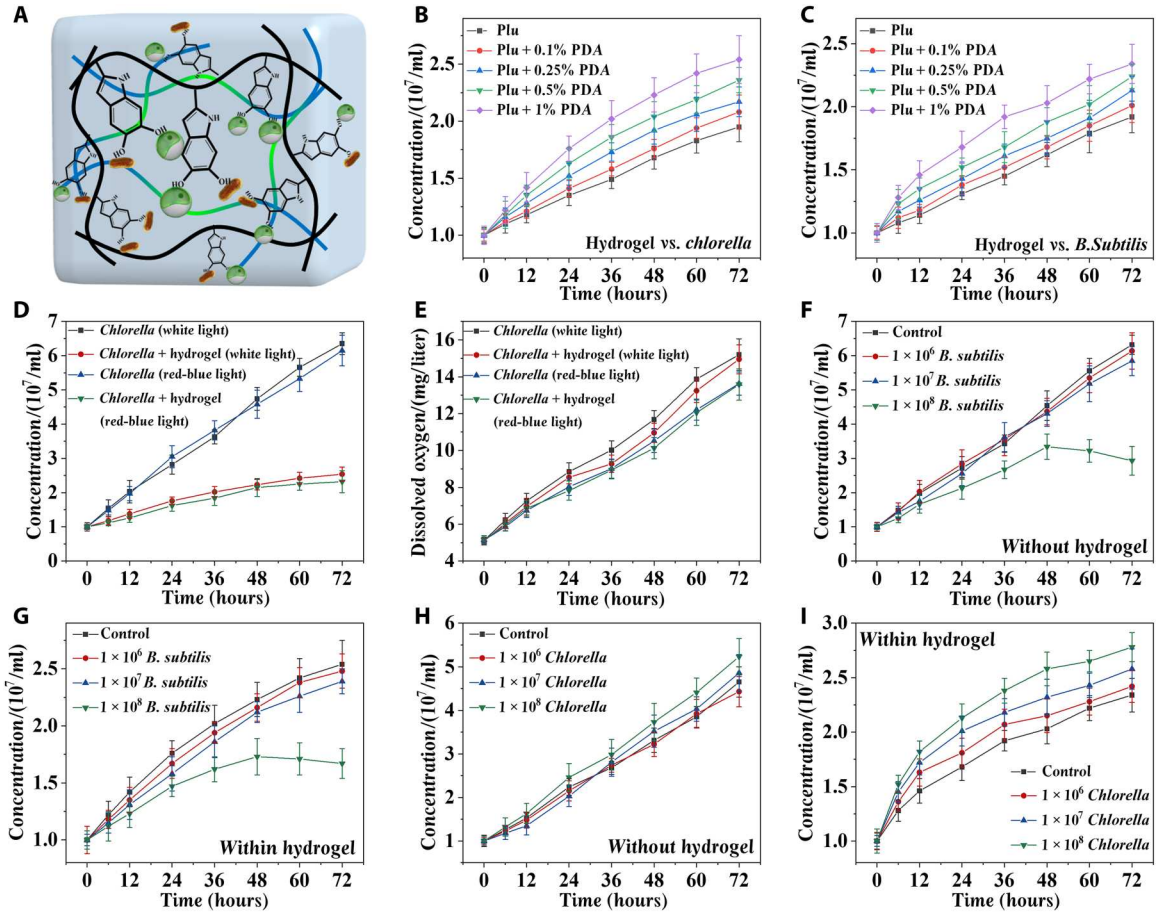

Fig. 3. Proliferation and dissolved-oxygen released capabilities of the LMH. (**A**) Schematic illustration and statistical analysis of F-127–PDA hydrogel for proliferation of *Chlorella* and *B. subtilis*. (**B**) Proliferation rate of the *Chlorella* in the hydrogel with 0.1, 0.25, 0.5, and 1% PDA added. (**C**) Proliferation rate of the *B. subtilis* in the hydrogel with 0.1, 0.25, 0.5, and 1% PDA added. (**D**) Proliferation rates of *Chlorella* under different kinds of lights with or without hydrogel encapsulation. (**E**) The amount of dissolved oxygen released from *Chlorella* under different kinds of lights with or without hydrogel encapsulation. The influence of concentrations of *B. subtilis* on the proliferation of *Chlorella* without (**F**) or within (**G**) hydrogel. The influence of concentrations of *Chlorella* on the proliferation of *B. subtilis* without (**H**) or within (**I**) hydrogel. $n = 3$ per group (B to I).

(HUVECs) and fibroblasts were used to identify the hypoxia relief capacity of LMH. The exposure with 1% O_2 was used to result in cell hypoxia. Considering the bacterial toxicity to cells, the living algae hydrogel (LAH) without *B. subtilis* encapsulation was used in this experiment. The effect of LAH on hypoxic L929 fibroblast viability was examined. The cell viability decreased notably in the state of hypoxia but remained high with the existence of LAH (light; Fig. 4, C and D), indicating that the dissolved oxygen released by *Chlorella* could substantially maintain the viability of hypoxic fibroblasts and further accelerate the regeneration of granulation tissue. In addition, the tube formation test was used to evaluate the effect of LAH on angiogenesis in hypoxic tissues. It was demonstrated that the tube formation process in the LAH (light)–treated group was notably increased in comparison with the hypoxia and hypoxia treated with LAH (dark) group (Fig. 4, E and F). It was indicated that the dissolved oxygen released from *Chlorella* could enhance the angiogenesis process in hypoxia status.

On the basis of the desirable oxygen-producing and antibacterial capabilities, the practical value of LMHs in treating chronic hard-to-heal wounds was evaluated. An *S. aureus*–infected full-thickness defect wound of a diabetic rat model with a diameter of about 1 cm was established. All rats were assigned into five groups at random and treated by phosphate-buffered saline (PBS), hydrogel, LAH, LBH, and LMH. The wound healing process in these groups was photographed over 9 days (Fig. 5, A and B). The chronic wounds treated by PBS underwent a slow healing process, and pus that formed by infection and hypoxia could be observed in the wound bed. However, the healing process in the chronic wounds treated with LAH, LBH, and LMH needed much less time, and almost no symptom of pus was observed. The substantially shorter healing periods of LAH, LBH, and especially LMH were further identified by the quantification of wound closure rates and thickness of regenerated granulation tissue (Fig. 5, C to E). In addition, as infection is the key factor affecting the wound healing process, the inflammatory factor interleukin-6 (IL-6) was stained to test the efficacy of LMH in controlling infections (fig. S14). A large amount of IL-6 was observed in the granulation tissue of the PBS-treated group after 9 days, while little secretion was detected in the LBH and LMH groups, suggesting that down-regulated inflammation response could be achieved. The amounts

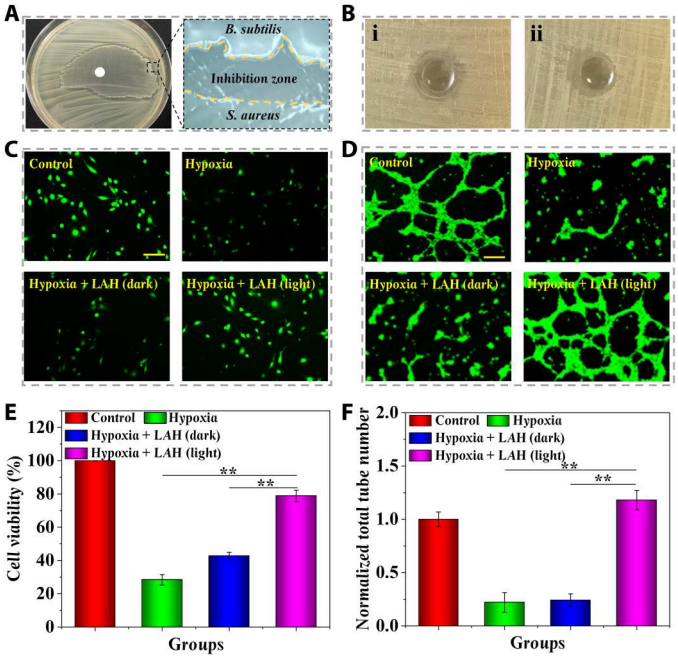

Fig. 4. Antibacterial and anti-hypoxia capabilities of the LMH. (**A**) Image of the inhibition zone formed between *B. subtilis* and *S. aureus*. (**B**) Inhibition zone formed by (i) LBH loaded with simple *B. subtilis* and (ii) LMH loaded with both *B. subtilis* and *Chlorella*. (**C**) Representative photographs of L929 fibroblasts that suffered from hypoxia in different treatments. (**D**) Representative photographs of the tube formation of HUVECs that suffered from hypoxia in different treatments. (**E**) Statistical analysis of the cell viability of L929 fibroblasts that suffered from hypoxia in different treatments. (**F**) Statistical analysis of the tube formation of HUVECs that suffered from hypoxia in different treatments. Scale bars, 200 μm (C and D). $n = 6$ per group (E and F). $^{**}P < 0.01$.

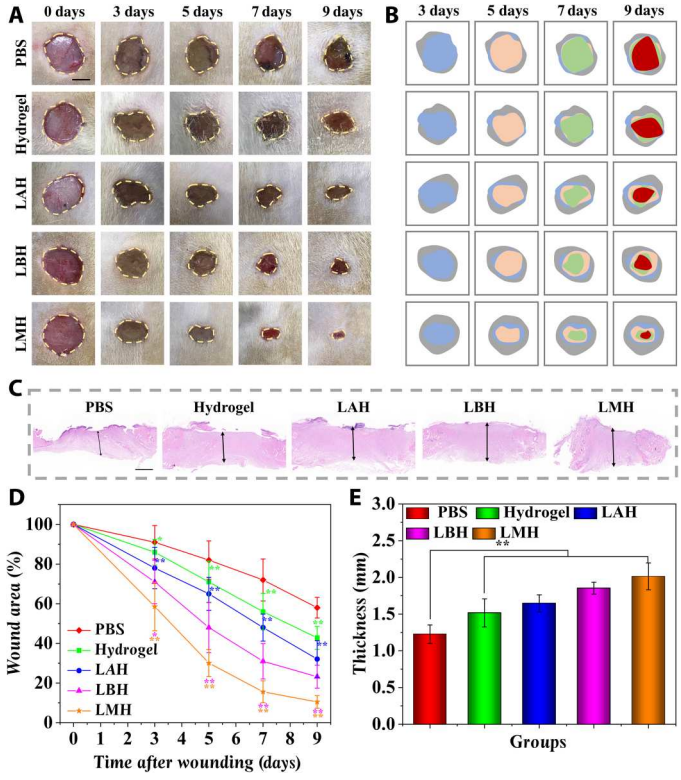

Fig. 5. The LMH accelerated the wound healing process of the infected diabetic wounds. (**A**) Representative images of full-thickness skin defect wounds treated by PBS, hydrogel, LAH, LBH, and LMH. (**B**) Schematic illustrations of the healing process of the wound bed. (**C**) The regenerated granulation tissues were stained by hematoxylin and eosin (H&E) staining after 9 days. (**D**) Quantification of the wound area healed by different treatments. (**E**) Quantification of granulation tissue thickness in different groups. Scale bars, 5 mm (A) and 1 mm (C). $n = 6$ per group. $^{*}P < 0.05$ and $^{**}P < 0.01$.

of bacterial loading in wound beds treated by LMH were further evaluated by in vivo imaging system (IVIS). A progressive infection was observed in the PBS-treated group, while the infection was quickly controlled in the LMH-treated group (fig. S15). This phenomenon may be ascribed to the antibacterial capability of the encapsulated *B. subtilis*.

To further explore the mechanism of LMH promoting chronic wound healing, the immunofluorescence staining of CD31 was tested to evaluate the angiogenesis process. More regenerated blood vessels could be observed in the LAH-, LBH-, and especially LMH-treated groups than in the PBS control and the hydrogel-alone group (Fig. 6, A and E). The enhanced neovascularization can offer more sufficient nutrient substance and oxygen supply for tissue regeneration and thus promote the wound healing process. In acute wounds, short-time hypoxia is beneficial to the angiogenesis process of wound healing. However, the continuous hypoxia in chronic wounds may lead to vascular atrophy and tissue necrosis. The immunohistochemistry staining of hypoxia-inducible factor 1α (HIF-1α) was tested to assess the degree of hypoxia in the granulation tissues. The presence of brown or brown particles in the nucleus or cytoplasm of HIF-1α protein is positive for staining, and the staining intensity indicates the positive degree. It was found that the expression of HIF-1α in LAH and LMH groups was obviously lower than that in the PBS, hydrogel, and LBH groups (Fig. 6, B and F). Hypoxia may affect the proliferation of repair cells and lead to the inactivation of various growth factors. The LMH could realize hypoxia relief by delivering dissolved oxygen into the wound bed, accelerating the healing procedure.

Secretion of extracellular matrix especially collagen is vital to promote wound healing; thus, Masson′s trichrome staining was conducted to characterize the degree of extracellular matrix deposition. Collagen was stained as blue, while the cytoplasm, muscle fibers, and red blood cells were stained as red. Few collagen depositions were observed in the PBS-treated group, while a large amount of collagen with tissue cell infiltration could be observed in the hydrogel, LAH, LBH, and especially LMH groups (Fig. 6, C and G). Collagen can serve as a scaffold for angiogenesis, cell migration, and granulation tissue regeneration. In addition, the phenotypic differentiation of fibroblasts into myofibroblasts also exhibits contractile property and play a major role in the contraction, traction, and maturation of granulation tissue. The double immunofluorescent staining of myofibroblast [stained by α–smooth muscle actin (α-SMA)] and fibroblasts (stained by vimentin) was performed to characterize the proportion of myofibroblast. It could be observed that more myofibroblasts existed in the granulation tissues of the LAH, LBH, and LMH groups (Fig. 6D), and denser tissue density could be observed.

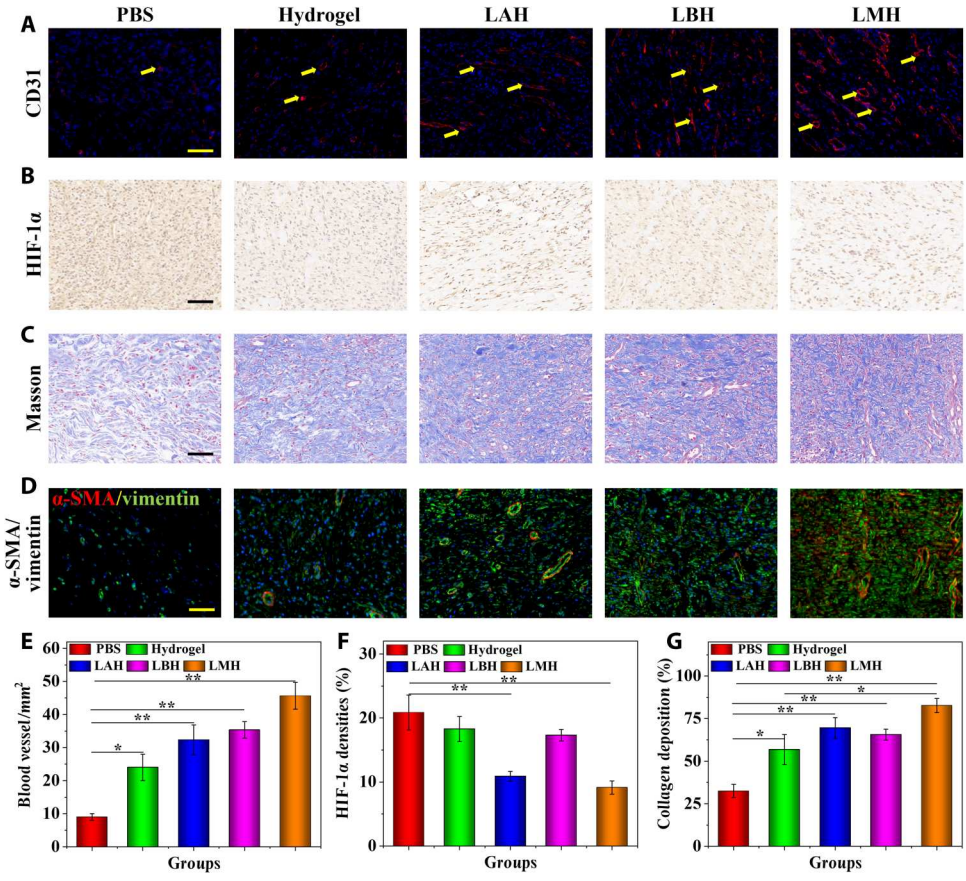

Fig. 6. The mechanism of LMH promoting chronic wound repair. (**A**) The CD31-positive blood vessel endothelial cells were stained as red. (**B**) Immunohistochemical staining of HIF-1α in granulation tissues in different groups. (**C**) Masson's trichrome staining of granulation tissues in different treatments. (**D**) Double immunofluorescence staining of α-SMA and vimentin of granulation tissues in different treatments. (**E** to **G**) Quantification of (E) blood vessel number, (F) HIF-1α densities, and (G) collagen deposition. Scale bars, 100 μm (A to D). $n = 6$ per group. $^{*}P < 0.05$ and $^{**}P < 0.01$.

The therapeutic effects of LMH on hard-to-heal wounds at 12 days were tested to observe the long-term effects. From the results of hematoxylin and eosin (H&E) and Masson's trichrome staining, the obvious epithelialization could be observed in the hydrogel, LAH, LBH, and LMH groups, especially the LMH group. The regenerated tissue in the LMH-treated group exhibited a structure similar to the normal tissue with epithelialization, hair follicle regeneration, and reticular collagen deposition (fig. S16). Compared to the results at 9 days, more blood vessels were regenerated in the granulation tissue at 12 days, showing more progressed wound repair (fig. S17, A and D). The degree of hypoxia and inflammation was further decreased at 12 days compared to the results of 9 days. The wound healing progress turned to the remolding phase at 12 days, during which the inflammation subsided, the collagen networks were arranged, and the tissue structure was remodeled. These results demonstrated that the LMH was ideal for promoting chronic wound healing through antibacteria, hypoxia relief, angiogenesis, collagen deposition, and fibroblast differentiation.

DISCUSSION

To conclude, inspired by the natural mechanism of oxygen-produced algae and more competitive bacteria against other microbes, we fabricated a thermosensitive, wet-adhesive hydrogel encapsulated with *Chlorella* and *B. subtilis* to form LMH for accelerating chronic hard-to-heal wound process. Benefiting from the thermosensitive Pluronic F-127, the LMH could quickly gel upon attaching the wound bed and could be easy to manage. The abundant catechol group in the mussel-inspired PDA further enhanced the adhesive force between LMH and the wound surface and promoted cellular proliferation of the encapsulated microorganism. After engraftment onto the wound bed, *Chlorella* could continuously release dissolved oxygen to relieve hypoxia degree in the wound bed and support the oxygen supply for the *B. subtilis* proliferation, while *B. subtilis* produced antibacterial agents to eliminate the pathogenic bacteria, reducing the infection degree and protecting the *Chlorella*. The healing process of the infected diabetic wound was substantially promoted by the LMH. These results demonstrated that the thermosensitive, wet-adhesive hydrogel with *Chlorella* and *B. subtilis* encapsulation was promising in treating hard-to-heal wounds and valuable for various disease treatments.

The clinical treatments of hard-to-heal wounds mainly include debridement, decompression, flap transplantation, negative pressure wound therapy, and external application of growth factors. Few existing methods can reverse the progress of chronic wounds. In particular, for the elderly, their body functions decline, the rate of

epidermal regeneration and amount of collagen deposition decreases, and they have difficulty tolerating surgical treatment, resulting in increasingly limited options for the treatment of chronic wounds. Therefore, it is urgent to develop novel effective therapies to overcome the challenge of clinical wound treatments. To date, living microbiological therapies have drawn more and more attention, including cells, bacteria, algae, etc. These therapies were developed in treating various clinical diseases and have achieved considerable therapeutic effects. Bacteria and algae with specific functions could be selected according to the demands of disease treatment. However, the functions of a single microorganism were relatively simple, and it is difficult to meet the complex commands of disease treatments. The combination of oxygen-producing *Chlorella* and antibacterial *B. subtilis* has not been investigated yet. In addition, the convenient formulations for clinical applications of these microorganisms were still deficient. Hence, we proposed the concept of LMH, aiming to integrate the distinctive advantages of different microorganisms and explore the strategy to realize their coexistence and mutually support. The wild types of microorganisms were selected in this study to exhibit their inherent promising capabilities. In the following studies, functions of the combined microorganisms can be enhanced to be more in line with the complex requirements of various disease treatments by gene editing technology, etc. It is anticipated that the development of living microecological therapy can offer more alternative choices and promote the progress of clinical disease treatment.

MATERIALS AND METHODS

Materials and cells

Pluronic F-127 and dopamine hydrochloride were obtained from Sigma-Aldrich. The *B. subtilis* 3610 and *S. aureus* (BNCC186335) were purchased from Bena Culture Collection.

The recombinant green fluorescent protein (GFP)–expressing *S. aureus* was obtained from the Department of Rheumatology and Immunology of Nanjing Drum Tower Hospital. The *Chlorella pyrenoidosa* and the corresponding algae culture medium were purchased from Nanjing Health Biotech.

The L929 fibroblasts were incubated in Dulbecco's modified Eagle's medium with the addition of 10% fetal bovine serum and 1% double antibiotics. The HUVECs were cultured in RPMI 1640 medium with the addition of 10% fetal bovine serum and 1% double antibiotics. The incubation temperature was set as 37°C, and the concentration of CO_2 was set as 5%.

Preparation of the LMH

Briefly, different concentrations of thermosensitive Pluronic F-127 (15, 16, 17, 18, 19, and 20%) were fabricated by dissolving the Pluronic F-127 powders in distilled water. The solutions were dropped onto the top of the 37°C plate, and gelation time was recorded by observing the morphology. In addition, the PDA solution was fabricated by dissolving the dopamine hydrochloride in NaOH (pH 8) solution to settle down the final concentrations of 0.1, 0.25, 0.5, and 1%. Afterward, a corresponding dose of Pluronic F-127 powder was added to the PDA solution under low temperature to obtain the Pluronic F-127/PDA hydrogel. A similar process was followed for the 18% Pluronic F-127/1% PDA solution loaded with *B. subtilis* and *Chlorella* to fabricate the LMH. Their gelation times were tested to evaluate the effects of the addition of PDA, bacteria, and algae. The storage modulus was measured from 4° to 45°C at the constant shear strain of 1% and the frequency of 1 rad s^{-1}.

Adhesion test

The adhesion force was tested by a self-made device (fig. S18). The device was placed in an incubator with a temperature of 37°C. The glass slide was fixed on the Helipath Stand, and 50 μl of hydrogel at 4°C was dropped onto the center of the slide and equilibrated for 5 min. The pigskin was fixed on the lower end of the columella ($r = 0.5$ cm) with glue and then placed on the hydrogel. A weight (5 g) was placed on the columella for 5 min, and the device was balanced. Afterward, water was dropped to the beaker at a constant speed (5 ml/min) until the pigskin and hydrogel were separated, and the water mass was counted. The adhesion force was calculated by using the formula

$$f = 0.98\ m/\pi r^2 \quad (1)$$

where m is the mass of water and r is the radius of the columella.

Bacteria and algae viability assay

To evaluate the impacts of the addition of PDA on the proliferation ability, the *B. subtilis* (1×10^7) or *Chlorella* (1×10^7) were dispersed in the hydrogel with different concentrations of PDA, and its proliferation rates were tested at specific time nodes within 72 hours. To evaluate the influences of light sources on the proliferation ability, the white light light-emitting diode (LED) and the red-blue light LED were used to offer the illumination. The luminous intensity was set as 6000 lux, which was appropriate for the *Chlorella* growth. The proliferation rates of the *Chlorella* in solution and hydrogel were both tested. To evaluate the mutual effects of *B. subtilis* and *Chlorella* on proliferation ability, different concentrations of bacteria and algae were mixed in the solution or hydrogel, and their proliferation rates were tested.

Dissolved oxygen release test

The dissolved oxygen released from *Chlorella* in solution or loaded in the LMH was tested by the oxygen microsensor at 0, 6, 12, 24, 48, and 72 hours under white or red-blue light illumination at 37°C.

Antibacterial test

The representative *S. aureus* was used to evaluate the antibacterial capacity of LMH. The *S. aureus* was suspended in a PBS solution with a turbidity of 0.5 according to McFarland standard. Afterward, 50 μl of the *S. aureus* suspension was inoculated to the nutrition agar plates. The standard discs with a diameter of 6 mm loaded with 1×10^7 *B. subtilis*, LBH, and LMH were put onto the center of the plates. All of their diameters were set as 6 mm. After incubation for 24 hours at 37°C, the widths of the inhibition zones were taken down and counted. To further identify the antibacterial capacity of LMH on *S. aureus*, the *S. aureus* were suspended in the PBS solution with a turbidity of 0.5, and 10 μl of the suspension was diluted 100 times. The *S. aureus* was cocultured with the LMH through a transwell system for 3 days. One hundred microliters of the suspension was spread on the nutrition agar plates after 1, 2, and 3 days of coculture. The bacterial colonies were photographed and counted after 24 hours of culture at 37°C.

Hypoxia relief test

The L929 fibroblasts were implanted into the 24-well plate at the concentration of 1×10^5 cells per well for 24 hours to allow cell attachment. The concentration of O_2 was down-regulated to 1% to induce hypoxia. The LAH was cocultured with the cells through a transwell system. The control group was cultured in normal condition. The hypoxia group was cultured under 1% O_2 for 6 hours. The hypoxia + LAH (dark) group was cocultured with LAH under 1% O_2 but without light illumination. The hypoxia + LAH (light) group was cocultured with LAH under 1% O_2 and light illumination. The cells were stained with Calcein-AM to observe cell viability and photographed by microscopy (Olympus IX71).

The HUVECs were seeded in the 24-well plate coated by Matrigel matrix with a concentration of 5×10^4 cells per well. The experimental procedure was similar to the above, and the tube formation number was observed.

Establishment of the infected diabetic wound model

The 8- to 12-week-old male Sprague-Dawley (SD) rats were from the Drum Tower Hospital. All animal experimental protocols had been approved by the Animal Investigation Ethics Committee of the Drum Tower Hospital and conducted in line with the *Guide for the Care and Use of Laboratory Animals*. The rats were fated for 12 hours before modeling. The streptozotocin was dissolved in citrate buffer (pH 4.5) at the concentration of 2% (w/v) and then immediately injected into the abdominal cavity of SD rats with a dose of 70 mg/kg to induce type I diabetes mellitus. Five days later, blood glucose of each rat was tested, and more than 16.7 mM was considered as a successful model and used in subsequent experiments. Afterward, the rats were anesthetized by inhaled anesthesia with isoflurane, and their hair was shaved off the backs. A round, full-thickness skin defect (1 cm in diameter) was sheared on the back, and then, 200 μl of *S. aureus* solution (1×10^8 CFU/ml) was injected to induce infections.

In vivo infected diabetic wound treatment of the LMH

The rats were equivalently divided into five groups at random and treated with PBS, hydrogel, LAH, LBH, and LMH. Afterward, the rats were kept in single cages for 9 days. The dressings were placed onto the wound bed and covered by a medical transparent membrane. The dressings were changed every day, and the wound bed was rinsed after the removal of the dressings. The situation of the wounds was photographed and measured on days 0, 3, 5, 7, and 9. At 9 days, all the animals were euthanized, and the regenerated granulation tissues were cut out and immersed in 10% neutral formaldehyde.

Afterward, the samples were dehydrated and embedded in paraffin for examination. The microtome was used to cut the samples into slices with a thickness of 5 μm. The resultant sections were used for H&E and Masson's trichrome staining. To evaluate the angiogenesis process, the sections were reacted with primary antibody CD31 overnight at 4°C and then washed and incubated with tetramethylrhodamine isothiocyanate (TRITC) to conjugate secondary antibodies. The 4, 6-diamidino-2-phenylindole (DAPI) was used to label nuclei after rinsing and mounting the sections. To test the proportion of myofibroblast, sections were reacted with primary antibodies α-SMA and vimentin overnight at 4°C. Sections were washed and incubated with TRITC and fluorescein isothiocyanate to conjugate secondary antibodies. The nuclei were stained by DAPI. The sections for immunohistochemical staining were stained with HIF-1α.

The therapeutic effects of LMH on infected diabetic wounds were further evaluated at 12 days. The experimental methods were the same as above. The IVIS was used to evaluate the in vivo antibacterial capability of LMH. A 200-μl GFP-expressing *S. aureus* solution (1×10^8 CFU/ml) was injected to induce infections. Bacterial loading in the wound treated by PBS or LMH was tested by IVIS in the first 3 days. The wound bed was removed intact from the back, and then, the black card with a hole was used to cover the wound bed to eliminate fluorescent interference from hair. The excitation wavelength was set as 480 nm, and the emission wavelength was set as 520 nm. The representative fluorescence images at each time point were photographed.

Supplementary Materials

This PDF file includes:

Figs. S1 to S18

REFERENCES AND NOTES

1. S. Maschalidi, P. Mehrotra, B. N. Keçeli, H. K. L. De Cleene, K. Lecomte, R. Van der Cruyssen, P. Janssen, J. Pinney, G. van Loo, D. Elewaut, A. Massie, E. Hoste, K. S. Ravichandran, Targeting SLC7A11 improves efferocytosis by dendritic cells and wound healing in diabetes. *Nature* **606**, 776–784 (2022).
2. D. M. Peterson, W. E. Damsky, M. D. Vesely, Fever, hypotension, and a worsening necrotic wound. *JAMA* **327**, 1496–1497 (2022).
3. S. Yun, V. Greco, From start to finish-a molecular link in wound repair. *Science* **375**, 619–620 (2022).
4. K. Minton, IL-17A–HIF1α axis in epithelial wound repair. *Nat. Rev. Immunol.* **22**, 532–533 (2022).
5. V. Falanga, R. R. Isseroff, A. M. Soulika, M. Romanelli, D. Margolis, S. Kapp, M. Granick, K. Harding, Chronic wounds. *Nat. Rev. Dis. Primers* **8**, 50 (2022).
6. J. Wang, D. Huang, H. Yu, Y. Cheng, H. Ren, Y. Zhao, Developing tissue engineering strategies for liver regeneration. *Eng. Regen.* **3**, 80–91 (2022).
7. N. Tang, R. Zhang, Y. Zheng, J. Wang, M. Khatib, X. Jiang, C. Zhou, R. Omar, W. Saliba, W. Wu, M. Yuan, D. Cui, H. Haick, Highly efficient self-healing multifunctional dressing with antibacterial activity for sutureless wound closure and infected wound monitoring. *Adv. Mater.* **34**, e2106842 (2022).
8. Y. Qian, Y. Zheng, J. Jin, X. Wu, K. Xu, M. Dai, Q. Niu, H. Zheng, X. He, J. Shen, Immunoregulation in diabetic wound repair with a photoenhanced glycyrrhizic acid hydrogel scaffold. *Adv. Mater.* **34**, e2200521 (2022).
9. J. Ouyang, X. Ji, X. Zhang, C. Feng, Z. Tang, N. Kong, A. Xie, J. Wang, X. Sui, L. Deng, Y. Liu, J. S. Kim, Y. Cao, W. Tao, In situ sprayed NIR-responsive, analgesic black phosphorus-based gel for diabetic ulcer treatment. *Proc. Natl. Acad. Sci. U.S.A.* **117**, 28667–28677 (2020).
10. S. Crunkhorn, Promoting efferocytosis heals diabetic wounds. *Nat. Rev. Drug Discov.* **21**, 491 (2022).
11. L. Jin, X. Guo, D. Gao, C. Wu, B. Hu, G. Tan, N. du, X. Cai, Z. Yang, X. Zhang, NIR-responsive MXene nanobelts for wound healing. *NPG Asia Mater.* **13**, 24 (2021).
12. P. Konieczny, Y. Xing, I. Sidhu, I. Subudhi, K. P. Mansfield, B. Hsieh, D. E. Biancur, S. B. Larsen, M. Cammer, D. Li, N. X. Landén, C. Loomis, A. Heguy, A. N. Tikhonova, A. Tsirigos, S. Naik, Interleukin-17 governs hypoxic adaptation of injured epithelium. *Science* **377**, eabg9302 (2022).
13. N. J. Bernard, IL-17A heals wounds. *Nat. Immunol.* **23**, 1134 (2022).
14. FLOW Investigators, M. Bhandari, K. J. Jeray, B. A. Petrisor, P. J. Devereaux, D. Heels-Ansdell, E. H. Schemitsch, J. Anglen, G. J. D. Rocca, C. Jones, H. Kreder, S. Liew, P. McKay, S. Papp, P. Sancheti, S. Sprague, T. B. Stone, X. Sun, S. L. Tanner, P. Tornetta, T. Tufescu, S. Walter, G. H. Guyatt, A trial of wound irrigation in the initial management of open fracture wounds. *New. Engl. J. Med.* **373**, 2629–2641 (2015).
15. M. Londahl, Hyperbaric oxygen therapy as treatment of diabetic foot ulcers. *Diabetes Metab. Res.* **28**, 78–84 (2012).
16. Y. Wang, J. Li, X. Li, J. Shi, Z. Jiang, C. Y. Zhang, Graphene-based nanomaterials for cancer therapy and anti-infections. *Bioact. Mater.* **14**, 335–349 (2022).

17. W. Liu, R. Gao, C. Yang, Z. Feng, W. Ou-Yang, X. Pan, P. Huang, C. Zhang, D. Kong, W. Wang, ECM-mimetic immunomodulatory hydrogel for methicillin-resistant Staphylococcus aureus-infected chronic skin wound healing. *Sci. Adv.* **8**, eabn7006 (2022).
18. S. Y. Kang, A. Pokhrel, S. Bratsch, J. J. Benson, S. O. Seo, M. B. Quin, A. Aksan, C. Schmidt-Dannert, Engineering *Bacillus subtilis* for the formation of a durable living biocomposite material. *Nat. Commun.* **12**, 7133 (2021).
19. X. C. Wang, C. Y. Yang, Y. R. Yu, Y. J. Zhao, In situ 3D bioprinting living photosynthetic scaffolds for autotrophic wound healing. *Res. China* **2022**, 9794745 (2022).
20. J. Frenkel, W. Vyverman, G. Pohnert, Pheromone signaling during sexual reproduction in algae. *Plant J.* **79**, 632–644 (2014).
21. M. V. Berlanga-Clavero, C. Molina-Santiago, A. M. Caraballo-Rodríguez, D. Petras, L. Díaz-Martínez, A. Pérez-García, A. de Vicente, V. J. Carrión, P. C. Dorrestein, D. Romero, Bacillus subtilis biofilm matrix components target seed oil bodies to promote growth and anti-fungal resistance in melon. *Nat. Microbiol.* **7**, 1001–1015 (2022).
22. F. Cerullo, S. Filbeck, P. R. Patil, H. C. Hung, H. Xu, J. Vornberger, F. W. Hofer, J. Schmitt, G. Kramer, B. Bukau, K. Hofmann, S. Pfeffer, C. A. P. Joazeiro, Bacterial ribosome collision sensing by a MutS DNA repair ATPase paralogue. *Nature* **603**, 509–514 (2022).
23. K. T. Chou, D. Y. D. Lee, J. G. Chiou, L. Galera-Laporta, S. Ly, J. Garcia-Ojalvo, G. M. Süel, A segmentation clock patterns cellular differentiation in a bacterial biofilm. *Cell* **185**, 145–157.e13 (2022).
24. J. He, W. Ding, W. Han, Y. Chen, W. Jin, X. Zhou, A bacterial strain Citrobacter W4 facilitates the bio-flocculation of wastewater cultured microalgae Chlorella pyrenoidosa. *Sci. Total Environ.* **806**, 151336 (2022).
25. H. Li, J. Yao, R. Duran, J. Liu, N. Min, Z. Chen, X. Zhu, C. Zhao, B. Ma, W. Pang, M. Li, Y. Cao, B. Liu, Toxic response of the freshwater green algae Chlorella pyrenoidosa to combined effect of flotation reagent butyl xanthate and nickel. *Environ. Pollut.* **286**, 117285 (2021).
26. Q. Cao, W. Sun, T. Yang, Z. Zhu, Y. Jiang, W. Hu, W. Wei, Y. Zhang, H. Yang, The toxic effects of polystyrene microplastics on freshwater algae Chlorella pyrenoidosa depends on the different size of polystyrene microplastics. *Chemosphere* **308**, 136135 (2022).
27. A. M. Vieira, F. Zahed, A. C. Crispim, E. de Souza Bento, R. F. O. França, I. O. Pinheiro, L. A. Pardo, B. M. Carvalho, Production of levan from *Bacillus subtilis* var. *natto* and apoptotic effect on SH-SY5Y neuroblastoma cells. *Carbohydr. Polym.* **273**, 118613 (2021).
28. M. Krajnc, P. Stefanic, R. Kostanjšek, I. Mandic-Mulec, I. Dogsa, D. Stopar, Systems view of *Bacillus subtilis* pellicle development. *NPJ Biofilms Microbiomes* **8**, 25 (2022).
29. G. Fu, J. Yue, D. Li, Y. Li, S. Y. Lee, D. Zhang, An operator-based expression toolkit for Bacillus subtilis enables fine-tuning of gene expression and biosynthetic pathway regulation. *Proc. Natl. Acad. Sci. U.S.A.* **119**, e2119980119 (2022).
30. H. Dong, W. Liu, H. Zhang, X. Zheng, H. Duan, L. Zhou, T. Xu, R. Ruan, Improvement of phosphate solubilizing bacteria Paenibacillus xylanexedens on the growth of Chlorella pyrenoidosa and wastewater treatment in attached cultivation. *Chemosphere* **306**, 135604 (2022).
31. L. Zhang, Y. Xiang, H. Zhang, L. Cheng, X. Mao, N. An, L. Zhang, J. Zhou, L. Deng, Y. Zhang, X. Sun, H. A. Santos, W. Cui, A biomimetic 3D-self-forming approach for microvascular scaffolds. *Adv. Sci. (Weinh)* **7**, 1903553 (2020).
32. Y. Wang, L. Lu, G. Zheng, X. Zhang, Microenvironment-controlled micropatterned microfluidic model (MMMM) for biomimetic in situ studies. *ACS Nano* **14**, 9861–9872 (2020).
33. W. Li, L. S. Mille, J. A. Robledo, T. Uribe, V. Huerta, Y. S. Zhang, Recent advances in formulating and processing biomaterial inks for vat polymerization-based 3D printing. *Adv. Healthc. Mater.* **9**, e2000156 (2020).
34. Y. T. Wang, L. R. Shang, Y. J. Zhao, L. Y. Sun, Microfluidic generation of multicomponent soft biomaterials. *Engineering* **13**, 128–143 (2022).
35. X. Han, M. Sun, B. Chen, Q. Saiding, J. Zhang, H. Song, L. Deng, P. Wang, W. Gong, W. Cui, Lotus seedpod-inspired internal vascularized 3D printed scaffold for bone tissue repair. *Bioact. Mater.* **6**, 1639–1652 (2021).
36. Y. Zhang, J. Tu, D. Wang, H. Zhu, S. K. Maity, X. Qu, B. Bogaert, H. Pei, H. Zhang, Programmable and multifunctional DNA-based materials for biomedical applications. *Adv. Mater.* **30**, e1703658 (2018).
37. W. Yuan, Z. Li, X. Xie, Z. Y. Zhang, L. Bian, Bisphosphonate-based nanocomposite hydrogels for biomedical applications. *Bioact. Mater.* **5**, 819–831 (2020).
38. C. M. Shao, Y. X. Liu, J. J. Chi, F. F. Ye, Y. J. Zhao, Hierarchically inverse opal porous scaffolds from droplet microfluidics for biomimetic 3D cell co-culture. *Engineering* **7**, 1778–1785 (2021).
39. G.-L. Ying, N. Jiang, S. Maharjan, Y.-X. Yin, R.-R. Chai, X. Cao, J.-Z. Yang, A. K. Miri, S. Hassan, Y. S. Zhang, Aqueous two-phase emulsion bioink-enabled 3D bioprinting of porous hydrogels. *Adv. Mater.* **30**, e1805460 (2018).
40. C. Yin, X. Li, G. Wen, B. Yang, Y. Zhang, X. Chen, P. Zhao, S. Li, R. Li, L. Wang, C. S. Lee, L. Bian, Organic semiconducting polymer amphiphile for near-infrared-II light-triggered phototheranostics. *Biomaterials* **232**, 119684 (2020).
41. J. Yan, Y. Wang, M. Ran, R. A. Mustafa, H. Luo, J. Wang, J. H. Smått, J. M. Rosenholm, W. Cui, Y. Lu, Z. Guan, H. Zhang, Peritumoral microgel reservoir for long-term light-controlled triple-synergistic treatment of osteosarcoma with single ultra-low dose. *Small* **17**, e2100479 (2021).
42. L. Cai, D. Xu, H. Chen, L. Wang, Y. Zhao, Designing bioactive micro−/nanomotors for engineered regeneration. *Eng. Regen.* **2**, 109–115 (2021).
43. Y. Wang, Z. Zhang, H. Chen, H. Zhang, H. Zhang, Y. Zhao, Bio-inspired shape-memory structural color hydrogel film. *Sci. Bull.* **67**, 512–519 (2022).
44. P. Piewngam, Y. Zheng, T. H. Nguyen, S. W. Dickey, H. S. Joo, A. E. Villaruz, K. A. Glose, E. L. Fisher, R. L. Hunt, B. Li, J. Chiou, S. Pharkjaksu, S. Khongthong, G. Y. C. Cheung, P. Kiratisin, M. Otto, Pathogen elimination by probiotic *Bacillus* via signalling interference. *Nature* **562**, 532–537 (2018).

Acknowledgments

Funding: This work was supported by the National Key Research and Development Program of China (2020YFA0908200), the National Natural Science Foundation of China ((T2225003, 52073060 and 82203961), the Nanjing Medical Science and Technique Development Foundation (ZKX21019), the Clinical Trials from Nanjing Drum Tower Hospital (2022-LCYJ-ZD-01), Guangdong Basic and Applied Basic Research Foundation (2021B1515120054), and the Shenzhen Fundamental Research Program (JCYJ20190813152616459 and JCYJ20210324133214038). **Author contributions:** Conceptualization: Y.Z. Methodology: G.C. and F.W. Investigation: G.C., F.W., and X.Z. Visualization: G.C., F.W., X.Z., and Y.S. Supervision: Y.Z. Writing (original draft): G.C., F.W., and X.Z. Writing (review and editing): Y.S. and Y.Z. **Competing interests:** The authors declare that they have no competing interests. **Data and materials availability:** All data needed to evaluate the conclusions in the paper are present in the paper and/or the Supplementary Materials.

Submitted 17 December 2022
Accepted 18 April 2023
Published 24 May 2023
10.1126/sciadv.adg3478